Heat Spreading Revisited – Effective Heat Spreading Angle

Dirk Schweitzer and Liu Chen
Infineon Technologies AG
Am Campeon 1-12, 85579 Neubiberg, Germany
dirk.schweitzer@infineon.com

Abstract

There is probably no thermal engineer who has not yet developed his or her own spreadsheet to calculate the thermal resistance of a layered structure such as the chip / die-attach / lead-frame stack in a power semiconductor. The more sophisticated versions of such spreadsheets consider also the effect of heat-spreading inside the layers, usually assuming a constant spreading angle which is often chosen to be 45°. As simple as this approach is as poor are often the results compared to Finite Element simulations or measurements. Herein we propose a definition of the effective heat-spreading angle which is based on the local variation of the heat-flux density along the heat-flow path. Using this definition it is possible to accurately calculate the heat-spreading angle inside a given structure and thus to develop more accurate heat spreading models e.g. for spreadsheet calculations.

Keywords

Heat flux, heat spreading angle, Rth-JC.

1. Introduction

One of the most often used formulas in thermal engineering is probably the equation

$$R_{th} = \frac{\Delta x}{kA} \qquad (1)$$

for the thermal resistance R_{th} of a layer with thickness Δx, cross-sectional area A and thermal conductivity k. Assuming that the heat flow path inside a layered structure can be modeled by a series of truncated cones as shown in figure 1, thus taking into account the heat spreading, the total thermal resistance across this structure could be approximated using

$$R_{th} = \sum_i \frac{\Delta x_i}{k_i A_i}, \qquad (2)$$

Δx_i, A_i, k_i being thickness, cross-section, thermal conductivity, and specific heat of the i-th slice. In the following we will refer to this model by "truncated cone model" (TCM). Many spreadsheet calculations are based on it. However there are several problems with this approach:

1. The model assumes that the heat is spread homogeneously over the area A_i of each slice which is not true.
2. The model implicitly assumes that the temperature on all interfaces between any two slices is isotherm, i.e. that all isothermals are planar and parallel. Otherwise we would not be allowed to apply eq. (1) to calculate the partial resistance of each slice. Isothermal faces on both sides of a layer are in fact an (often forgotten about) pre-condition for the applicability of (1). But as any thermal engineer knows the isothermals in real structures are neither planar nor isothermal (figure 2).
3. The model assumes that the heat spreading angle ϕ is constant within each layer which is not true either as we will show below.
4. The model assumes that the heat spreading is independent from the external boundary conditions. As discussed in [1] and [2] and will be shown again below this is not the case either.

Therefore the results obtained using the truncated cone model and eq. (2) often deviate considerably from FE simulation results or measured R_{th} values and should be used with care. Additionally the heat-spreading angle ϕ within each layer is unknown. A value of 45° is often used but mostly based on our intuitive imagination of the heat spreading in a material with isotropic thermal conductivity; though some authors have investigated the applicability of the 45° heat spreading angle [3, 4].

In this paper we propose the definition of an effective heat spreading angle ϕ_{eff} which is based on the local variation of the heat-flux density $p(x)$ [W/mm^2] along the heat flow path. In combination with the truncated cone heat spreading model (TCM) as in figure 1 the use of the thus defined heat-spreading angle accurately reproduces the correct R_{th} of the structure.

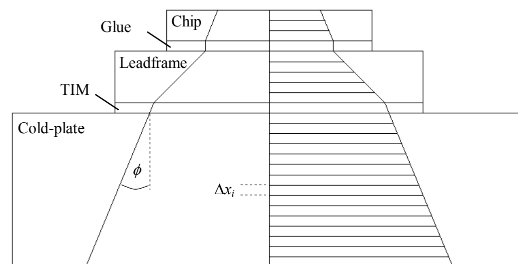

Figure 1: Simple heat spreading ("truncated cone") model for the calculation of the thermal resistance of a layered structure.

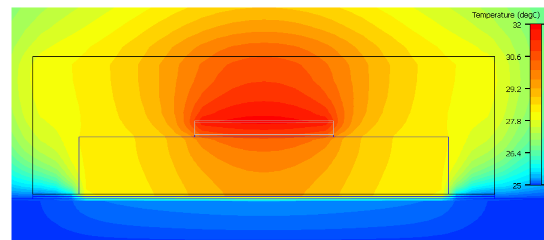

Figure 2: Non-planar isothermals in a real semi-conductor device.

2. Effective heat spreading angle

The concept of the effective heat spreading angle is quite simple. Instead of considering the heat flux distribution in the whole structure we focus on the local heat flux density $p(x)$ along the heat flow path and ask which heat spreading angle would result in the observed functional dependency $p(x)$ in a truncated cone model if assumptions 1+2 were true. In the following we consider the path Γ between the point of maximum temperature T_j on a semiconductor chip and the point of maximum case temperature T_c on the bottom side of the structure (figure 3). The heat source is located at $x = 0$ and the case surface at $x = x_{case}$.

A Finite Element simulation with sufficiently fine spatial resolution along the x-axis reveals the decrease of $p(x)$ along this path (figure 4). All parameters for that simulation are shown in table 1. The heat flux density decreases quickly throughout the silicon chip, it remains almost constant in the region of the glue die attach, and it slowly decreases further in the leadframe until it abruptly drops to zero at the case surface where a fixed temperature boundary condition was applied. Only an area A_0 = 1.0×1.0 mm² in the center of the 3.0×3.0 mm² chip surface was heated. The drop in heat flux density $p(x)$ is caused by heat spreading; therefore it seems reasonable to calculate the spreading angle based on $p(x)$ or the derivative dp/dx thereof.

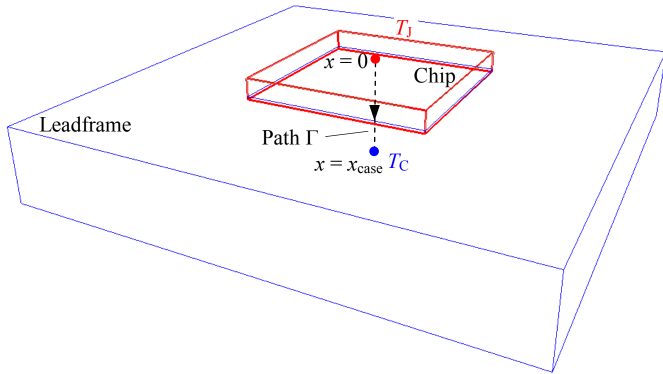

Figure 3: Path Γ along which the heat flux density $p(x)$ is monitored.

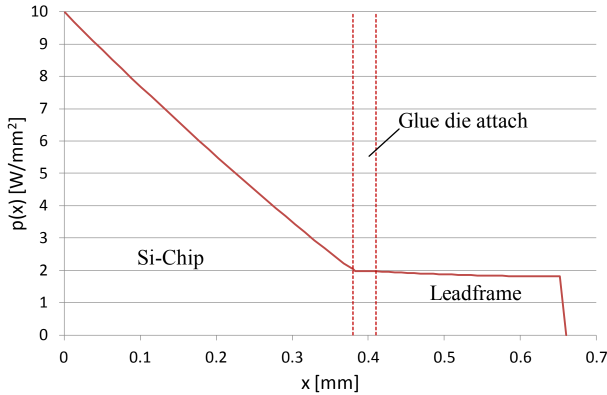

Figure 4: Heat flux density $p(x)$ along the path between junction and the case monitor point.

Layer	Material	Size [mm×mm×mm]	Thermal cond. [W/mK]
Chip	Silicon	3.0 × 3.0 × 0.38	148
Die attach	Glue	3.0 × 3.0 × 0.03	1.5
Leadframe	Cu alloy	6.0 × 6.0 × 0.25	350

Table 1: FE simulation model parameter: A power of 10W was dissipated homogenously on an active area A_0 = 1.0 × 1.0mm² on the surface of the chip, i.e. the initial heat flux density p_0 is 10 W/mm². At case a fixed temperature boundary condition is applied.

In the following we shall assume that the heat is always spread homogeneously over the whole area as in assumption (1) of the simple cone heat spreading model from figure 1. I.e. at depth x the heat is spread homogeneously over an *effective* area $A(x)$ which is given by

$$A(x) = A_0 \frac{p_0}{p(x)} \tag{3}$$

For a square area $A(x)$ its side length is

$$a(x) = \sqrt{A(x)} = a_0 \sqrt{\frac{p_0}{p(x)}}\,. \tag{4}$$

Plotting $y(x) = ½\, a(x)$ versus x we obtain the (upper half of the) heat spreading profile as shown in figure 5. The inclination of the tangent to that profile with respect to the horizontal is the effective heat spreading angle ϕ_{eff} at that point. It shall be emphasized again that the real heat spreading profile and angle will deviate somewhat from that in figure 5 because of

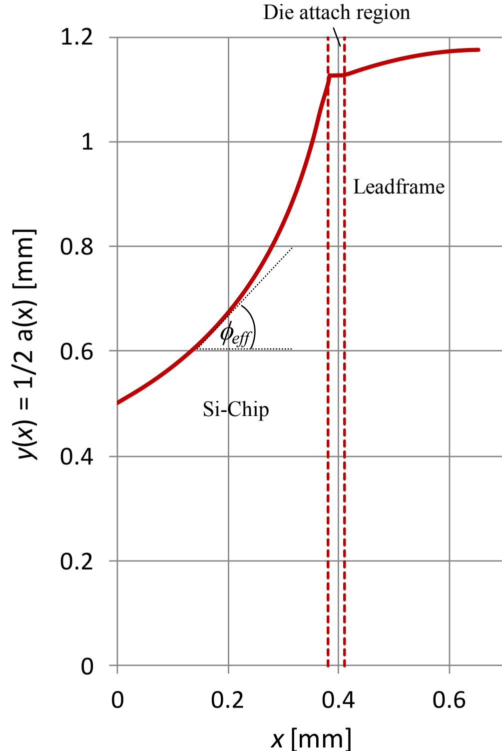

Figure 5: Effective heat spreading profile calculated for the heat flux density $p(x)$ from figure 4.

of the underlying assumptions (1) + (2) which are not met in reality. Therefore we call them *effective* heat spreading angle and *effective* heat spreading profile. But based on this profile we can construct a truncated cone heat spreading model which will exactly reproduce the true R_{th} of the layer structure because it correctly reproduces the heat flux density along the path between T_j and T_c. The temperature difference between start and end point of the heat flow path Γ is unambiguously defined by the heat flux density along that path:

$$\Delta T = \int_{\Gamma} \frac{p(x)}{k(x)} dx \cdot \tag{5}$$

3. Calculation of the effective heat spreading angle

If the heat flux is spread from an area $A(x)$ with circumference $L(x)$ to an area $A(x + dx)$ the area increases by

$$dA = L(x)\, dR \tag{6}$$

where $dR = dx \tan(\phi_{eff})$ (see figure 6). Taking the derivative of eq. (3) we obtain

$$\frac{dA}{dx} = -\frac{p_0 A_0}{p(x)^2} \frac{dp}{dx} \tag{7}$$

and from eq. (6) we know that

$$\frac{dA}{dx} = L(x)\frac{dR}{dx} = L(x)\tan(\phi_{eff}) \cdot \tag{8}$$

Therefore we obtain

$$\tan(\phi_{eff}) = -\frac{p_0 A_0}{L(x)} \frac{1}{p(x)^2} \frac{dp}{dx} \tag{9}$$

or, using again eq. (3),

$$\tan(\phi_{eff}) = -\frac{A(x)}{L(x)} \frac{1}{p(x)} \frac{dp}{dx} \tag{10}$$

for the effective spreading angle ϕ_{eff} at position x. This expression can be further evaluated for different shapes of the active area as shown in table 2 to obtain ϕ_{eff} solely as function of $p(x)$ and the derivative dp/dx thereof. In this concept the effective heat spreading angle seems to be a local quantity because it is derived solely from the local heat flux density. But $p(x)$ implicitly depends on the geometry, the material properties, and the boundary conditions of the whole structure and the effective heat spreading angle therefore reflects all these influencing factors.

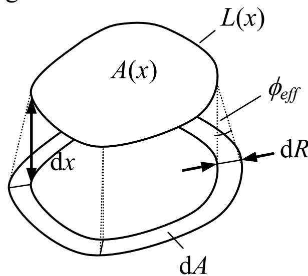

Figure 6: Heat spreading from area $A(x)$ to area $A(x + dx)$.

Active area	$\frac{A(x)}{L(x)}$	Effective heat spreading angle
Square, side a_0	$\frac{a(x)}{4}$	$\tan(\phi_{eff}) = -\frac{a_0}{4}\sqrt{\frac{p_0}{p(x)}}\frac{1}{p(x)}\frac{dp}{dx}$
Circle, radius r_0	$\frac{r(x)}{2}$	$\tan(\phi_{eff}) = -\frac{r_0}{2}\sqrt{\frac{p_0}{p(x)}}\frac{1}{p(x)}\frac{dp}{dx}$
Rectangle, aspect ratio $\beta = b_0/a_0$	$\frac{a(x)}{2(1+\frac{1}{\beta})}$	$\tan(\phi_{eff}) = -\frac{a_0}{2(1+\frac{1}{\beta})}\sqrt{\frac{p_0}{p(x)}}\frac{1}{p(x)}\frac{dp}{dx}$

Table 2: Formulas for the effective heat spreading angle for different shapes of the active area.

Figure 7 shows the resulting heat spreading angle $\phi_{eff}(x)$ for our example. Within the silicon chip the heat spreading angle increases from about 30° to 80°, contrary to the 45° spreading models. Within the glue die attach the heat spreading angle drops almost to zero. Within the leadframe the heat is initially spread with an angle of 22° which narrows down until the spreading angle becomes zero at the case side with fixed temperature boundary conditions. We will see in the next section that the heat spreading profile looks very different if we apply more realistic cooling conditions at the case side.

We see in the equations in table 2 that the effective heat spreading angle depends not only on the heat flux density $p(x)$ and its derivative but also on the dimension a_0 or r_0 of the active area: At first sight ϕ_{eff} seems to increase with the size of the active area which would be wrong since we can expect that the heat spreading originating from a larger area is lower. For an infinitely large planar heat source the spreading angle is in fact zero (one-directional heat-flow).

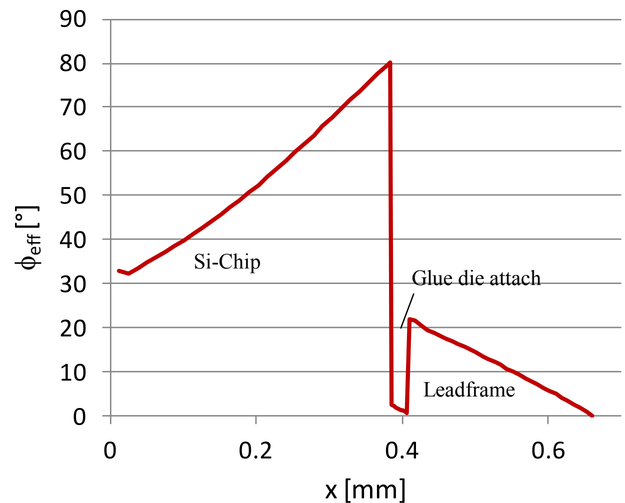

Figure 7: Effective heat spreading angle calculated for the heat flux density $p(x)$ from figure 4.

But if we keep the total power dissipation *P* constant, $p(x)$ does also decrease when a_0 or r_0 are increased, thus explaining the seemingly contradiction.

4. Influence of boundary conditions and device geometry

In this section we apply the concept of the effective heat spreading angle to visualize the influence of boundary conditions, material properties, and device geometry on the internal heat spreading of a power semiconductor device. For this purpose we consider again the three layer structure consisting of chip, die attach, and leadframe, as described in table 1.

4.1 Influence of the cooling condition at package case

First we want to demonstrate the influence of the external cooling condition. Figure 9 shows the effective heat spreading profile and angle inside the structure when different heat transfer coefficients are applied to its bottom (case) surface, namely: 5.0×10^3, 1.0×10^4, 5.0×10^4, 1.0×10^5W/(m^{2}K), and fixed case temperature, the latter corresponding to an infinitely high heat transfer coefficient. For comparison: data-sheet values for heat transfer coefficients of liquid cooled cold-plates range in between 5000 and 20000 W/(m^{2}K), whereas with liquid jet impingement values as high as 5.0×10^4 – 2.5×10^5 W/(m^{2}K) can be achieved [5]. While the cooling condition has almost no influence on the heat spreading inside silicon die and die attach we see a big impact of the boundary condition on the heat spreading inside the leadframe. The higher the heat transfer coefficient at the case surface the less the heat is spread inside the leadframe. For the fixed case temperature boundary condition finally, which can only be realized in simulations but is nevertheless often used to calculate the junction to case thermal resistance Rth-JC, the heat spreading behavior is fundamentally different: While for finite values of the heat transfer coefficient the spreading angle increases throughout the leadframe it is much lower for the fixed case temperature condition and even drops to zero at the case surface. These results underline once more the fact that heat spreading and consequently also the Rth-JC of a power semiconductor are influenced by the external boundary conditions (see also [2]).

4.2 Influence of die attach material properties

In the next step we investigate the influence of the die attach material, comparing thermally high conductive solder die attach (k = 53W/(mK)) to thermally low conductive glue die attach (k = 1.5W/(mK)). Again we use the structure from table 1 but increase for solder the thickness of the die attach from 30µm for glue to 50µm for solder. Figure 10 shows the resulting effective heat spreading profile and angle for glue (blue) and solder (red). We can see that the die attach has a big influence on the heat spreading inside the silicon chip. For glue die attach the heat is spread out much more inside the die than it is for solder die attach. A heat barrier, as represented by the thermally low conductive glue obviously causes the heat to spread out more in the preceding layer(s). If the Rth-JC is to be computed based on a truncated cone model (TCM) it is crucial to model the spreading inside the silicon chip correctly, especially so for thermally low conductive glue.

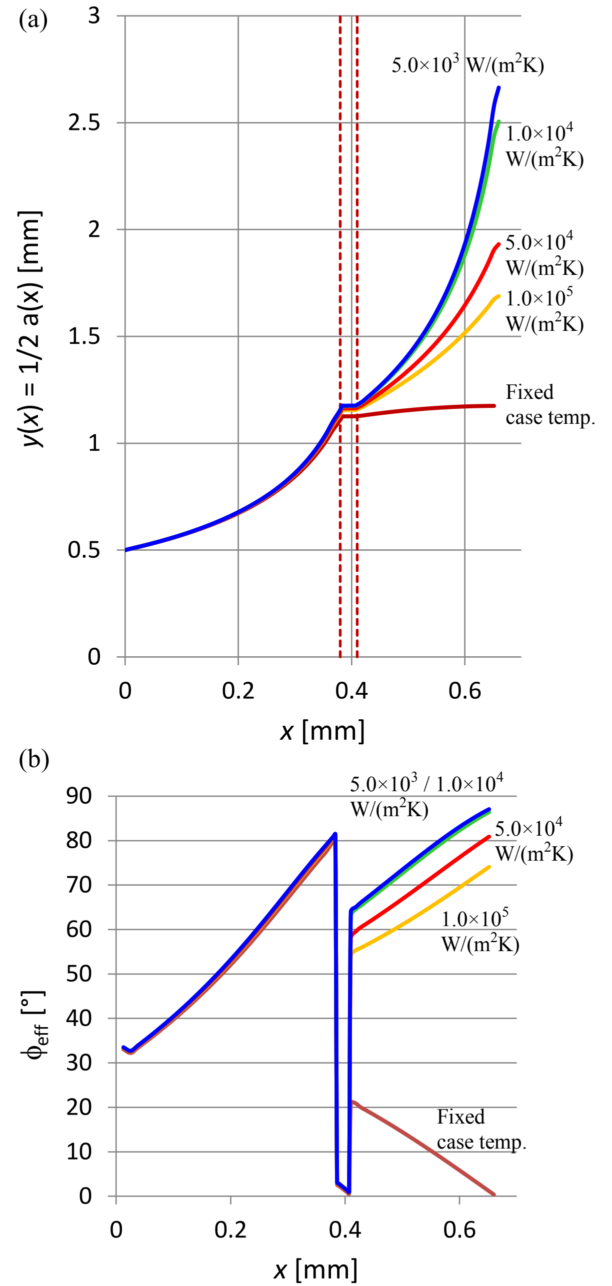

Figure 9: Effective heat spreading profile (a) and spreading angle (b) for different cooling conditions (heat transfer coefficients) at the case surface.

This is because the heat spreading inside the chip determines the cross sectional area of the heat flow through the die attach and therefore its thermal resistance. Despite its small thickness the die-attach often contributes a major part to the total thermal resistance of the device, since it is normally the material with the lowest thermal conductivity.

Not surprisingly the heat spreading inside the die attach is higher for solder than for glue due to its higher thermal conductivity. Inside the glue layer the spreading angle is close to zero. On the other hand the die attach has little influence on the heat spreading angle inside the leadframe which is only slightly larger for glue than for solder die attach (figure 10b).

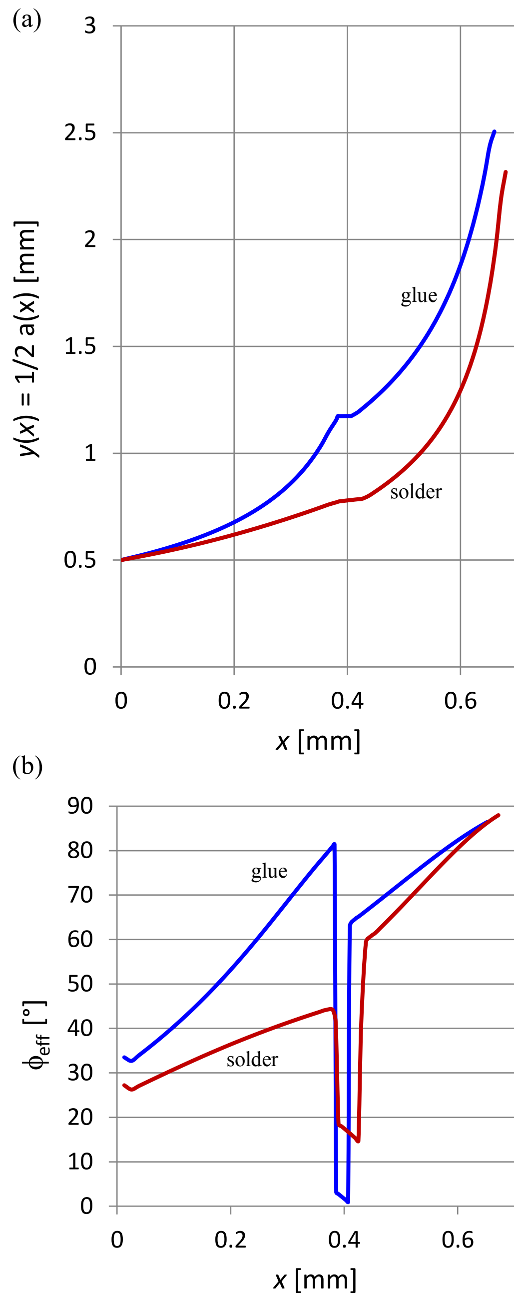

Figure 10: Effective heat spreading profile (a) and spreading angle (b) for glue and solder die attach. A heat transfer coefficient of $1.0{\times}10^4$ W/(m^{2}K) was applied at the case surface.

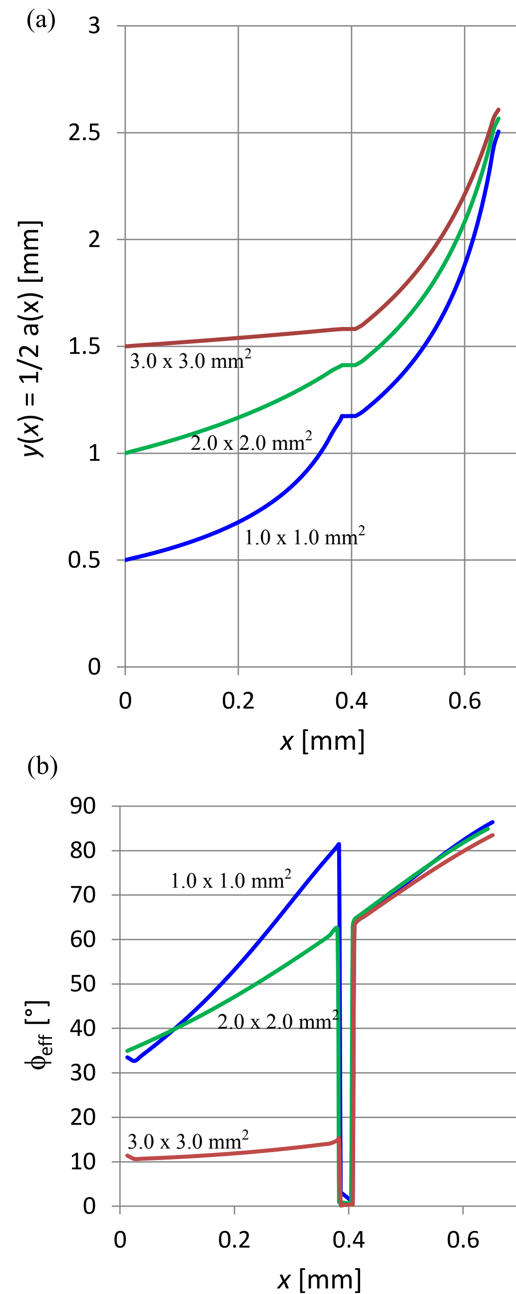

Figure 11: Effective heat spreading profile (a) and spreading angle (b) for different sizes of the active area. A heat transfer coefficient of $1.0{\times}10^4$ W/(m^{2}K) was applied at the case surface.

4.3 Influence of the size of active area

Finally we demonstrate the impact of the size of the active area on the chip over which the power is dissipated. For that purpose we increase the size of the active area on the 3.0 x 3.0 mm^2 chip of our test structure from 1.0 x 1.0 mm^2 to 2.0 x 2.0 mm^2 and 3.0 x 3.0 mm^2.

Figure 11 compares the resulting effective heat spreading profiles and spreading angles, revealing that the size of the active area has a major impact on the heat spreading. We observe that the heat spreading angle inside the chip decreases with increasing size of the active area.

Once the active area becomes equal to the chip size the heat spreading angle inside the chip drops to small values however not to zero which may be surprising at first. The subsequent leadframe which is larger than the chip provides plenty of room for lateral heat spreading which causes the heat flux lines to bend already inside the chip. This effect can also be observed in figure 2 where we see non-planar isothermals already in the chip, even so the whole surface of the die was heated homogeneously.

The heat spreading angle inside the copper leadframe on the other hand is not influenced by the size of the active area.

5. A practical example

In order to demonstrate the applicability of the effective heat spreading concept we use the method to calculate Rth-JC values for four power packages with exposed die pads of different leadframe thickness (figure 12). The Rth-JC of the same packages had previously been determined in a Finite Element simulation study using the detailed models shown in figure 12. Therefore accurate Rth-JC values are available for comparison. In the FE simulations a fixed case temperature boundary condition had been applied to determine Rth-JC.

To gain insight into the dependence of the heat spreading inside the leadframe on its thickness we performed a few simulations with our test structure (table 1) for different values of the leadframe thickness and with fixed case temperature, the results of which are shown in figure 13. We see that the heat spreading angle inside the leadframe starts at values from 25° to 45°, depending on its thickness, and that it decreases to zero towards the case surface due to the ideal cooling boundary condition.

Since we do not want to treat each leadframe thickness separately we decided to approximate this behavior by a heat spreading angle which starts at an average value of 35° and decreases linearly to zero towards the case surface. Furthermore we neglect the small amount of heat spreading inside chip and die attach, assuming zero heat spreading in that region. The resulting truncated cone model with a 4-slice discretization of the leadframe can be seen in figure 14. We implemented this TCM in a spreadsheet calculator as follows: The bottom side length a_i of the i-th slice of the leadframe heat spreading cone with square cross section and thickness d_i is

$$a_i = a_{i-1} + d_i \tan\phi_{i-1}, \quad a_0 = \sqrt{A_0} \qquad (11)$$

To compute the thermal resistance $R_{th,i}$ of each slice we use the area of the center plane

$$R_{th,i} = \frac{d_i}{k_i A_i}, \quad A_i = \frac{1}{4}(a_{i-1} + a_i)^2 . \qquad (12)$$

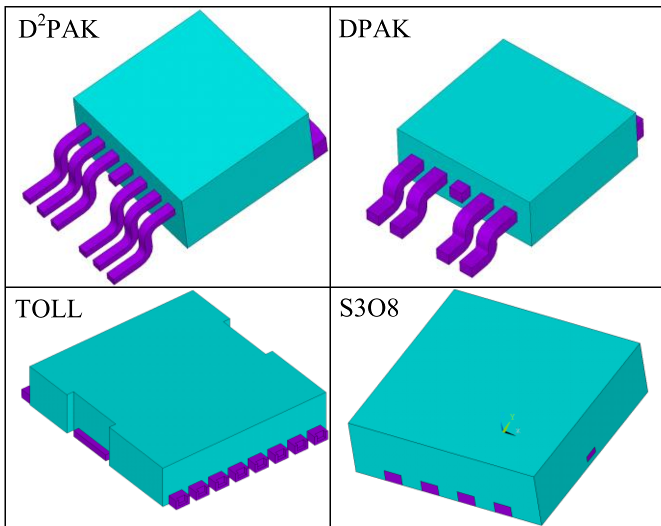

Figure 12: FE models of 4 power packages with exposed die-pad of different thickness.

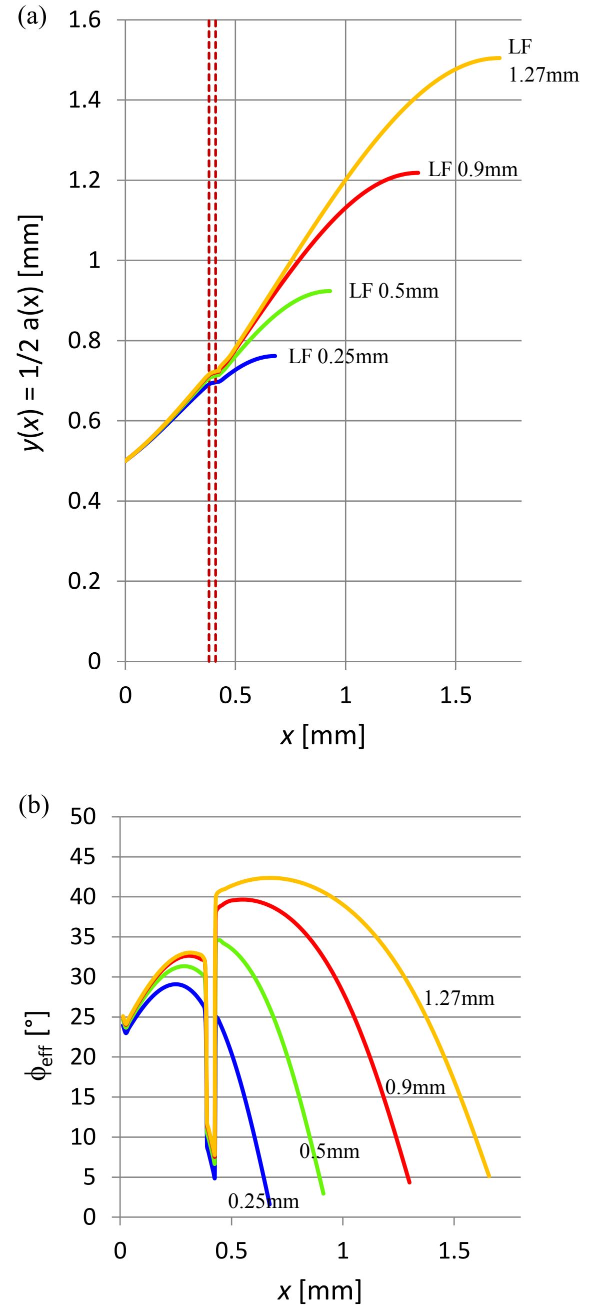

Figure 13: Effective heat spreading profile (a) and spreading angle (b) for the structure from table 1, but solder die attach and varying leadframe thickness. A fixed case temperature boundary condition was applied at package case.

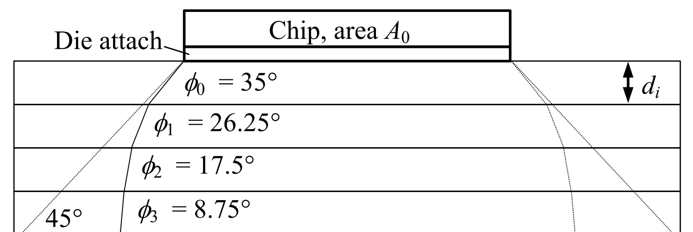

Figure 14: Truncated cone model used to calculate Rth-JC.

Package	LF Thickness	Chip size	(a) Rth-JC FEM simulation	(b) Rth-JC Effective heat spread. model	Error	(c) Rth-JC spreading angle 45°	Error
D^2PAK	1.27	1	1.802	1.942	7.77%	1.477	-18.04%
	1.27	2	1.116	1.139	2.06%	0.880	-21.15%
	1.27	4.5	0.620	0.592	-4.52%	0.472	-23.87%
	1.27	10	0.333	0.301	-9.61%	0.249	-25.23%
DPAK	0.9	1	1.717	1.757	2.33%	1.390	-19.04%
	0.9	2	1.033	0.996	-3.58%	0.805	-22.07%
	0.9	4.5	0.548	0.499	-8.94%	0.417	-23.91%
	0.9	10	0.280	0.246	-12.14%	0.213	-23.93%
TOLL	0.5	1	1.457	1.411	-3.16%	1.201	-17.57%
	0.5	2	0.835	0.761	-8.86%	0.663	-20.60%
	0.5	4.5	0.405	0.362	-10.62%	0.325	-19.75%
	0.5	10	0.189	0.171	-9.52%	0.158	-16.40%
SSO8	0.25	1	1.154	1.055	-8.58%	0.968	-16.12%
	0.25	2	0.597	0.547	-8.38%	0.510	-14.57%
	0.25	4.5	0.268	0.251	-6.34%	0.238	-11.19%
	0.25	10	0.121	0.115	-4.96%	0.111	-8.26%

Table 3: Comparison of the Rth-JC values computed using (a) detailed finite element models, (b) the effective heat spreading model, and (c) the 45° heat spreading model.

Since we do not assume heat spreading inside chip and die attach the corresponding layers need not to be subdivided. The Rth-JC values obtained by summation over the $R_{th,i}$ values of all slices of this model are listed in column (b) in table 3. For comparison we have also computed the Rth-JC values with the same TCM assuming a constant 45° heat spreading angle inside the leadframe in column (c). With respect to the Finite Element results in column (a) the error of effective heat spreading model is much smaller than that of the 45° heat spreading model which overestimates the spreading angle.

The thus validated spreadsheet could now be used to quickly calculate the Rth-JC for a wide range of different power packages with exposed die pad. However we have to keep in mind the assumptions for which the underlying heat spreading model has been derived; e.g. in this case we assumed ideal cooling and no heat spreading inside the die. For other cooling conditions or devices with a small active area on a larger die we would have to adapt the heat spreading model in our spreadsheet.

6. Conclusion

We propose the definition of an effective heat spreading angle ϕ_{eff} which is based on the local heat flux density $p(x)$ along a heat flow path. Based on this heat spreading angle and the associated heat spreading profile it is in principle possible to calculate the exact value of the temperature difference between start and end point of the path using a truncated cone heat spreading model (TCM).

For a single specific case there would be little motivation to do so since the calculation of $p(x)$ itself requires a Finite Element simulation which could as well be used to directly calculate the temperature difference. But as demonstrated in the previous example it is often possible to derive a heat spreading model for a wide enough range of applications to make it worth the effort. We hope that the results presented herein can help to solve the mystery of the “correct” heat spreading angle in numerous spread sheet calculators, hopefully resulting in more accurate estimates of Rth-JC and other thermal resistances.

References

1. C.J.M. Lasance, “Heat Spreading – Not a trivial Problem”, Electronics Cooling, Vol. 14, No. 2, May 2008.
2. Dirk Schweitzer, “The Junction-To-Case Thermal Resistance – A Boundary Condition dependent Thermal Metric”, Proc. 26th SEMI-THERM, Santa Clara, pp. 151-157, 2010.
3. Bruce Guenin, “The 45° Heat Spreading Angle – An Urban Legend?”, Electronics Cooling, Vol. 9, No. 4, Nov. 2003.
4. Yasushi Koito, Shoryu Okamoto, and Toshio Tomimura, “Two dimensional numerical investigation on applicability of 45° heat spreading angle”, Journal of Electronics Cooling and Thermal Control, Vol. 4, pp. 1-11, 2014.
5. T.A. Shedd, "Fundamental Behaviors and Limits of Impingement Cooling", Proc. 23th SEMITHERM, San Jose, pp. 179-183, 2007.